Available online at www.sciencedirect.com
ScienceDirect
Transactions of Nonferrous Metals Society of China
www.tnmsc.cn
Trans. Nonferrous Met. Soc. China 26(2016) 508−518

Deformation behavior and constitutive model for dual-phase Mg−Li alloy at elevated temperatures

Guo-bing WEI[1], Xiao-dong PENG[1], Fa-ping HU[1], Amir HADADZADEH[2], Yan YANG[1], Wei-dong XIE[1], Mary A. WELLS[2]

1. College of Materials Science and Engineering, Chongqing University, Chongqing 400044, China;
2. Mechanical and Mechatronics Engineering Department, University of Waterloo, Waterloo, ON, N2L 3G1, Canada

Received 9 March 2015; accepted 27 July 2015

Abstract: In order to study the deformation behavior and evaluate the workability of the dual-phase Mg−9Li−3Al−2Sr alloy, isothermal hot compression tests were conducted using the Gleeble−3500 thermal-mechanical simulator, in ranges of elevated temperatures (423−573 K) and strain rates (0.001−1 s^{-1}). Plastic instability is evident during the deformation which is in the form of serrated flow; serrated yielding is attributed to the locking of mobile dislocations by the Mg and Li atoms which diffuse during the deformation. The relationships between flow stress, strain rate and deformation temperature were analyzed and the deformation activation energy and some basic material factors at different strains were calculated using the Arrhenius equation. The effects of temperature and strain rate on deformation behavior were represented using the Zener−Hollomon parameter in an exponent-type equation. To verify the validity of the constitutive model, the predicted values and experimental flow curves under different deformation conditions were compared, the correlation coefficient (0.9970) and average absolute relative error (AARE=4.41%) were calculated. The results indicate that the constitutive model can be used to accurately predict the flow behavior of dual-phase Mg−9Li−3Al−2Sr alloy during high temperature deformation.

Key words: constitutive model; Mg−Li alloy; plastic instability; Zener−Hollomon parameter

1 Introduction

Mg alloys are considered to be one of the lightest metallic materials for structural applications in sectors such as transportation and aerospace owing to their low density, high specific strength and high damping capacity [1−4]. However, traditional magnesium alloys such as AZ31 and AZ91 alloys have poor formability and limited ductility ascribed to their hexagonal close-packed (HCP) crystal structure [5,6]. On the other hand, Mg−Li alloys with good formability and low density are attracting more and more attention in both industry and research [7,8]. According to the Mg−Li binary phase diagram, Mg alloys with Li content of 5.5%−11.5% exhibit a duplex phase structure of α-Mg (HCP) and β-Li (BCC) phases [9]. Mg−Li alloys have excellent cold-formability compared with other Mg-based alloys due to the decrease of c/a axial ratio as well as the formation of the BCC structure with the addition of Li [9]. But, Mg−Li alloys exhibit low mechanical strength which is not beneficial for structural applications. Hence, it is important to improve the mechanical properties of Mg−Li alloys while still maintaining its ductility. For most magnesium products, plastic deformation techniques such as rolling, forging and extrusion are employed to refine the grain size and enhance the strength. Moreover, adding alloying elements is another beneficial method to improve the strength with both solution hardening and precipitation hardening techniques, such as Al, Zn, rare earth elements (Y, La and Ce) and alkaline earth elements (Sr,Ca) [10−13]. Aluminum (Al) is the most widely used alloying element in strengthening of Mg−Li alloys by means of solid solution and intermetallic compound reinforcements. But when the Al content is greater than 3% in Mg−Li−Al alloys, the elongation of alloys starts to decrease [14,15]. The alkaline earth element Sr is often added into Mg−Li−Al alloys to improve the mechanical properties, the metallic compound Al_4Sr distributed in β-Li phase

Foundation item: Projects (CDJZR14130007, 106112015CDJXY130011) supported by Fundamental Research Funds for the Central Universities, China
Corresponding author: Xiao-dong PENG; Tel/Fax: +86-23-65111625; E-mail: pxd@cqu.edu.cn
DOI: 10.1016/S1003-6326(16)64139-0

can strengthen the Mg−Li alloy effectively [9,16]. For instance, by adding Al and Sr to a Mg−Li alloy it was observed that extruded Mg−9Li−3Al−2Sr alloy exhibits favorable mechanical properties due to grain refinement and dispersion strengthening [9].

To assess the hot formability of Mg−Li alloys, knowledge of the material flow stress at elevated temperatures is important. Development of constitutive models for different temperatures and strain rates provides quantitative data that can be used to numerically analyze the hot forming processes using techniques such as the finite element method (FEM) [17]. The flow stress at elevated temperatures is usually dependent on the deformation temperature, strain, strain rate and chemical composition of the material [18,19]. Many researchers have used the flow stress to develop the constitutive equation for a variety of Mg alloys. HU and JU [20] researched Anand's model of AZ31 magnesium alloy based on the hot compression test and simulated twin-roll thin strip casting process. The constitutive law was developed for AZ31B-H24 Mg alloys and finite element analysis was offered for advanced superplastic analysis on AZ31 Mg alloys [21]. Some of Mg alloys studied by different constitutive models included Mg−Zn−Cu−Zr alloy [22], Mg−2.0Zn−0.3Zr alloy [23], ZK60 alloy [24] and short-fiber-reinforced magnesium matrix composite [25].

The microstructure evolution in hot deformation will also provide information that can help to optimize the optimal process parameters for hot working. However, review of the published literature shows that few analytical studies have been done to measure or analyze the flow stress and deformation behavior of the duplex Mg−Li alloys at elevated temperatures. The extruded Mg−9Li−3Al−2Sr alloy exhibits a favorable combination of strength and ductility with an ultimate tensile strength of 235 MPa and an elongation of 19.4% at room temperature, and would be an alternative material for engineering [9]. The objective of this study is to measure the flow behavior of Mg−9Li−3Al−2Sr alloys at high temperatures and establish a suitable constitutive equation that correlates the deformation temperature and strain rate to flow stress as a function of strain. Knowledge of this will help to design and optimize hot deformation processes for these alloys.

2 Experimental

Commercial purity Mg, Li and Al (>99.9%) were used to prepare the alloys used in this study. Sr was added in the form of an Al−10Sr master alloy. Before melting, all materials were polished to remove surface oxide. The charge was melted in a resistance furnace under an argon atmosphere. After melting, the melt was held at 950 K for 0.5 h and then poured into a stainless mold (60 mm in diameter and 120 mm in height). The ingot was homogenously treated at 573 K for 4 h in a vacuum furnace. The actual chemical composition of the alloy was measured by induction coupled plasma (ICP-AES) and test results are shown in Table 1. Compression samples (d10 mm × 15 mm) were taken from the ingot by a machining lathe and grinder machine. According to the XRD pattern in Fig. 1, the Mg−9Li−3Al−2Sr alloy is mainly composed of α-Mg, β-Li, Al_4Sr and a small quantity of $Mg_{17}Al_{12}$ phases. The optical micrograph of the as-cast Mg−9Li−3Al−2Sr alloy is shown in Fig. 2. The typical duplex phase structure of α-Mg with HCP structure and β-Li with BCC structure can be easily observed. As shown in Fig. 2, the dark areas are the β-Li matrix phase while the bright or light areas are the α-Mg phases with random orientation.

Table 1 Chemical composition of Mg−9Li−3Al−2Sr alloy (mass fraction, %)

Item	Li	Al	Sr	Mg
Nominal	9	3	2	Bal.
Actual	8.92	2.98	2.04	Bal.

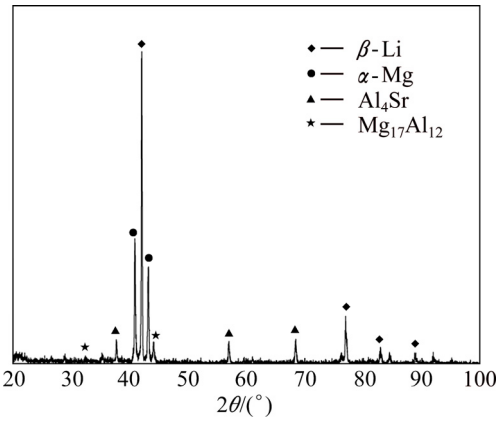

Fig. 1 XRD pattern of as-cast Mg−9Li−3Al−2Sr alloy

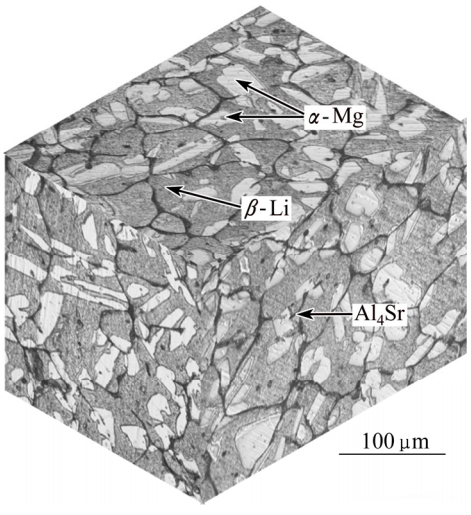

Fig. 2 Optical micrograph of as-cast Mg−9Li−3Al−2Sr alloy

The Al_4Sr phases are mainly distributed in the β-Li phase.

According to the standard ASTM E9, the hot compression tests were performed on the Gleeble−3500 thermal-mechanical simulator. The specimens were heated with a rate of 10 K/s and held at the deformation temperature for 20 s to obtain a constant sample temperature before deformation. The temperatures of the specimens were recorded and controlled using thermocouples attached to the surface of the specimens at the mid-width position. The compression tests were done at temperatures of 423, 473, 523 and 573 K with strain rates of 1, 0.1, 0.01, 0.001 s^{-1} to a true strain of 0.6. After deformation, the specimens were quenched with water for 10 s so that the as hot-deformed microstructure could be observed. The load displacement data were measured and recorded during the isothermal compression by a computer connected to the Gleeble machine with an automatic data acquisition system and subsequently changed to true stress−true strain data.

3 Results and discussion

3.1 Stress−strain behavior and microstructure evolution

The stress−strain data obtained from the hot compression tests under different strain rate and temperature conditions can be used to determine the material constants for a constitutive model that can then be used to predict the stress−strain response of the material under different temperature, strain rate and strain conditions. [18,26]. Typical true stress–strain curves for this alloy are shown in Fig. 3. By increasing the deformation temperature or decreasing the strain rate, the overall level of flow stress curve decreases. In the initial stage of the deformation, the stress increases sharply and reaches a peak stress at a low strain level. After the peak stress, the flow stress decreases gradually, indicating that dynamic flow softening occurs as the hot deformation progresses. This phenomenon indicates that the compression process of Mg−9Li−3Al−2Sr alloy is a dynamic competition procedure between the work-hardening and caused by dynamic recovery and dynamic recrystallization [23]. The α-Mg and β-Li phases are compressed as shown in Fig. 4**.** Twinning is the dominate deformation mode for the α-Mg phases in the process of hot working at low temperatures (423−473 K) and high strain rates. The continuous Al_4Sr phases were broken into particles and mainly distributed in the β-Li matrix during the deformation. As shown in Fig. 5, the dynamic recrystallization of β-Li phases is the main mechanism of work softening. The fine DRX grains formed at original

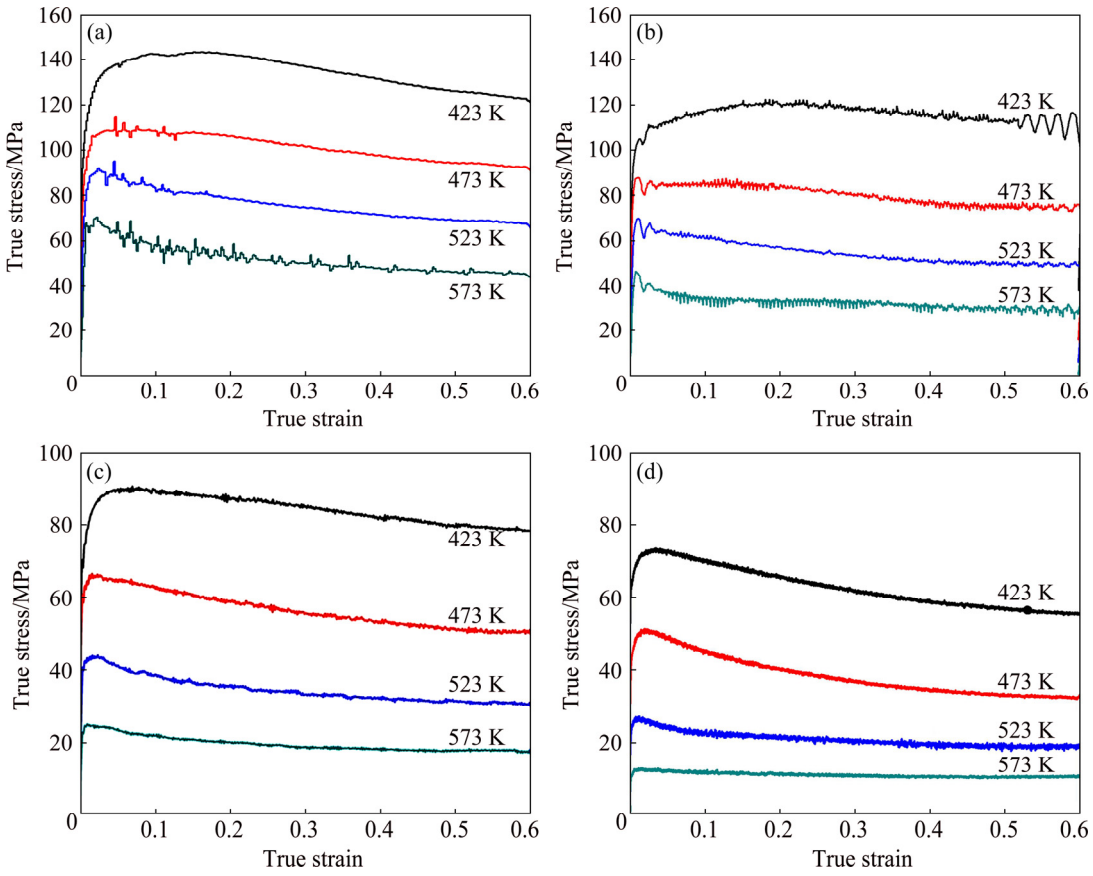

Fig. 3 True stress−strain curves of Mg−9Li−3Al−2Sr alloy treated at different deformation temperatures with strain rates 1 s^{-1} (a), 0.1 s^{-1} (b), 0.01 s^{-1} (c) and 0.001 s^{-1} (d)

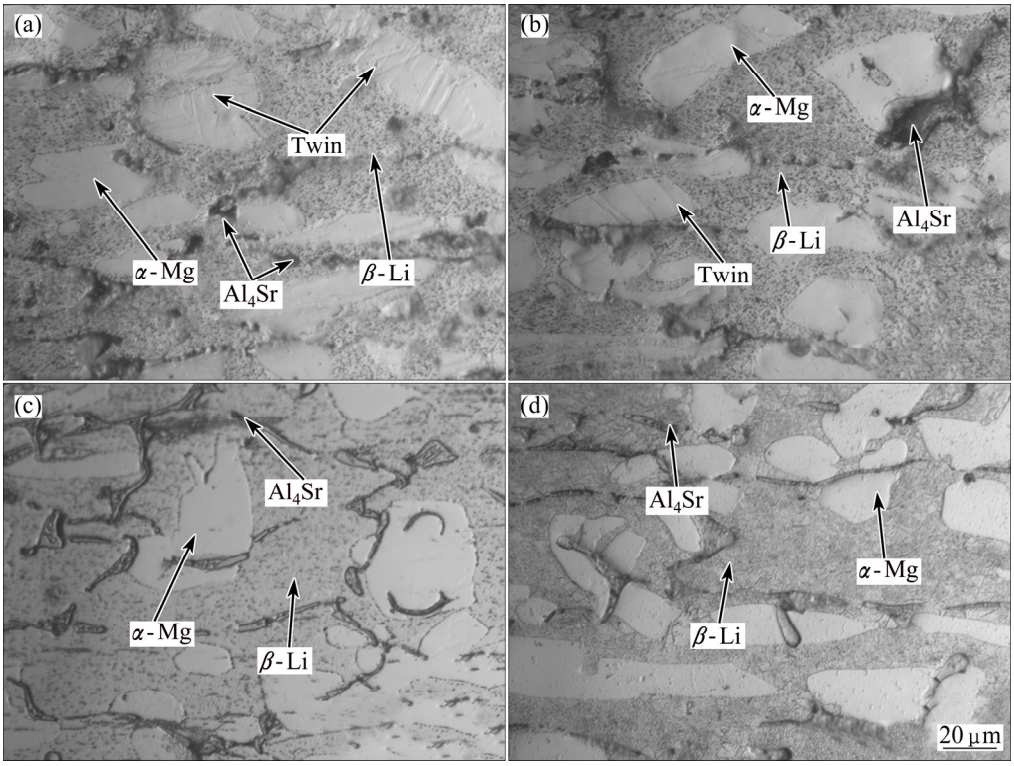

Fig. 4 Optical micrographs of Mg−9Li−3Al−2Sr alloy treated with strain rate of 1 s^{-1} at different deformation temperatures: (a) 423 K; (b) 473 K; (c) 523 K; (d) 573 K

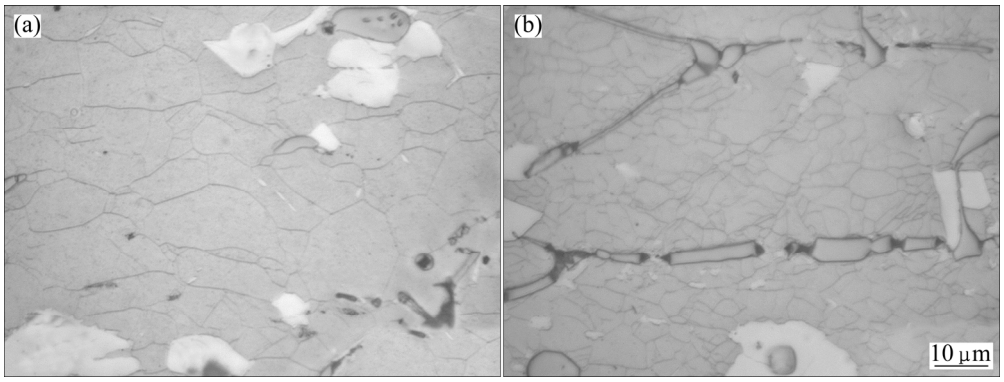

Fig. 5 Optical micrographs of Mg−9Li−3Al−2Sr alloy treated at 523 K and different strain rates: (a) 0.1 s^{-1}; (b) 1 s^{-1}

grain boundaries and around the Al_4Sr particles because the dislocation of high density is first developed in the vicinity of coarse original grains boundaries and the interface between matrix and second phase particles [27].

Plastic instability, in the form of serrated flow occurs at strain rates of 1−0.1 s^{-1} as shown in Fig. 3. Outside this strain rate range, smooth flow curves were obtained for this alloy. For a strain rate of 1 s^{-1}, the alloy exhibited obvious serrations of periodic fluctuation in the flow curves except at 423 K. NIE et al [28] observed the same behavior for Mg−Gd(−Mn−Sc) alloy where serrated flow occurred when the alloy was deformed at temperatures of 423−523 K rather than lower temperatures (RT−373K) or higher temperature (623 K) at a fixed strain rate. NIE et al [29] reported that the Mg−Y−Nd alloy exhibits flow serrations when deformed at temperatures of 423−498 K. The temperature ranges where serrated flow is observed are 513−558 K for Mg−Th alloys and 326−397 K for Mg−Ag alloys [30]. The occurrence of flow serration is closely linked to the deformation temperature. The occurrence of serrated flow increases with increasing the temperature at a strain rate of 1 s^{-1}, as shown in Fig. 3(a). The serration segments of the flow curves at different deformation temperatures deformed at a strain rate of 0.1 s^{-1} are presented in Fig. 3(b). Smooth flow curves were observed at strain rates of 0.01 and 0.001 s^{-1}, respectively. The effect of strain rate on serrated flow

was also reported for Mg−Y−Nd, Mg−Li−Al and Mg−Gd(−Mn−Sc) alloys [28,29,31].

The serrated flow also known as jerky flow or the PLC (Portevin-Le Chatelier) effect, was mainly observed for Al alloys or single phase Mg alloys in the tensile test at elevated temperatures [32]. This phenomenon in dual-phase Mg−Li alloy during compression test is seldom reported. CHATURVEDI et al [30] reported that three mechanisms give rise to serrated flow: dislocation/solute-atom interaction, dislocation/precipitate reaction and twinning. Deformation twins can be seen at low temperatures referring to Figs. 4(a) and (b) in deformed samples. On the other hand, serrated flow occurred at high temperatures for strain rate of 1 s^{-1} while the twins were not observed (Figs. 4(c) and (d)). Thus, twinning may be responsible for small irregularities at low temperatures during compression test, while it is not the main reason of the serrations observed at higher temperatures [30].

COTTRELL [33] proposed the phenomenon of dynamic strain aging (DSA); the solute atoms pin and unpin gliding dislocations repeatedly which then lead to the serrations. DSA is generally a phenomenon observed in ductile alloys at elevated temperatures, and the Mg−Li alloy with reasonably good formability is presented in this group. WANG et al [32] studied serrated flow in Mg−4Li−1Al (LA41) alloy during tensile testing through the competition between dynamic strain aging (DSA) of solute atoms and shearing of precipitates by dislocations. Since serration flow mainly occurred at high strain rates of 1 and 0.1 s^{-1} in this alloy, the serrated flow can be interpreted as follows. In the dual-phase Mg−9Li−3Al−2Sr alloy, the solute atoms Mg and Li can be considered as obstacles relative to dislocations. At high strain rates, the dislocations accumulate significantly in a short period of time. The solute atoms can intercept and create drag on the mobile dislocations during the deformation, then the velocity of the dislocations is reduced suddenly and the dislocations become temporarily "locked", this represents the onset of serrated yielding [32]. The "locked" dislocations might accumulate as the deformation continues, when the velocity of the dislocation is greater than the obstacles, the arrested dislocations will be set free, causing the flow stress to decrease simultaneously [30,32]. Such behavior will repeat automatically during the test and the true strain–stress curves will show the periodicity of the serrated flow macroscopically. But at low strain rates, the density of dislocation is low and relatively easy to dissipate, so the amplitude of serration flow is smaller at strain rate of 0.1 s^{-1}. The serration flow did not occur at strain rates of 0.01 and 0.001 s^{-1} in a short time, because the motion of the Mg or Li atoms was not fast enough towards moving dislocations and needed a certain time at a given temperature [34,35].

3.2 Establishing and validating constitutive model

In order to express the relationship among the strain rate, flow stress and temperature, the Arrhenius equation has been widely applied for the warm and hot deformation of the aluminum and magnesium alloys [23,36]. The combined effect of temperature and strain rate on the deformation behavior can be expressed by the Zener–Hollomon parameter (Z), as shown in Eq. (1). Using the Zener−Hollomon parameter the deformation activation energy (Q) of the alloy can be determined [26,37]. In metallic materials, Eq. (2) is used to describe the relationship between the strain rate and flow stress. The hot deformation conditions under which the different constitutive equations applied are provided in Eq. (3) [38].

$$Z = \dot{\varepsilon}\exp[Q/(RT)] \tag{1}$$

$$\dot{\varepsilon} = AF\sigma\exp[-Q/(RT)] \tag{2}$$

$$F\sigma = \begin{cases} \sigma^{n'}, & \alpha\sigma < 0.8 \\ \exp(\beta\sigma), & \alpha\sigma > 1.2 \\ [\sinh(\alpha\sigma)]^{n}, & \text{for all } \sigma \end{cases} \tag{3}$$

where $\dot{\varepsilon}$ is the strain rate; R is the mole gas constant; T is the thermodynamic temperature; Q is the hot deformation activation energy; σ is the flow stress for a given stain; A, α, β, n and n' are the material constants which are independent of temperature. The relationship among α, β and n' can be expressed as [26]

$$\alpha = \frac{\beta}{n'} \tag{4}$$

By substituting Eq. (3) into Eq. (2), the functional relation between flow stress and strain rate can be described for low stress levels ($\alpha\sigma$<0.8), high stress levels ($\alpha\sigma$>1.2) and all conditions of stress, using Eqs. (5)−(7), respectively [37]:

$$\dot{\varepsilon} = A_1\sigma^{n'} \tag{5}$$

$$\dot{\varepsilon} = A_2\exp(\beta\sigma) \tag{6}$$

$$\dot{\varepsilon} = A[\sinh(\alpha\sigma)]^{n}\exp[-Q/(RT)] \tag{7}$$

where A, A_1 and A_2 are the temperature-independent material constants. By assuming that deformation activation energy (Q) is not a function of temperature T, and taking the natural logarithm on both sides of Eqs. (5)−(7) respectively, the following equations will be obtained:

$$\ln\dot{\varepsilon} = \ln A_1 + n'\ln\sigma \tag{8}$$

$$\ln\dot{\varepsilon} = \ln A_2 + \beta\sigma \tag{9}$$

$$\ln\dot{\varepsilon}=\ln A-\frac{Q}{RT}+n\ln[\sinh(\alpha\sigma)] \tag{10}$$

The strain−stress curves with strain rates of 1 s^{-1} and 0.1 s^{-1} were fitted to reduce the fluctuations and smooth the data as shown in Fig. 6. A strain of 0.2 was taken as an example to introduce the evaluation procedure of the material constants. The values of n' and β can be obtained from the slope of the lines in $\ln\dot{\varepsilon}-\ln\sigma$ and $\ln\dot{\varepsilon}-\sigma$ plots according to Eqs. (8) and (9), respectively, as seen in Fig. 7. By taking the mean values of the fitted slopes in Fig. 7, n'=6.33 and β=0.117 were obtained. Then, $\alpha=\beta/n'$=0.01848 using Eq. (4). Taking partial derivatives of both sides of Eq. (10), the following equation can be derived [39]:

$$Q=R\left\{\frac{\partial\ln\dot{\varepsilon}}{\partial\ln[\sinh(\alpha\sigma)]}\right\}_T\left\{\frac{\partial\ln[\sinh(\alpha\sigma)]}{\partial(1000/T)}\right\}_{\dot{\varepsilon}} \tag{11}$$

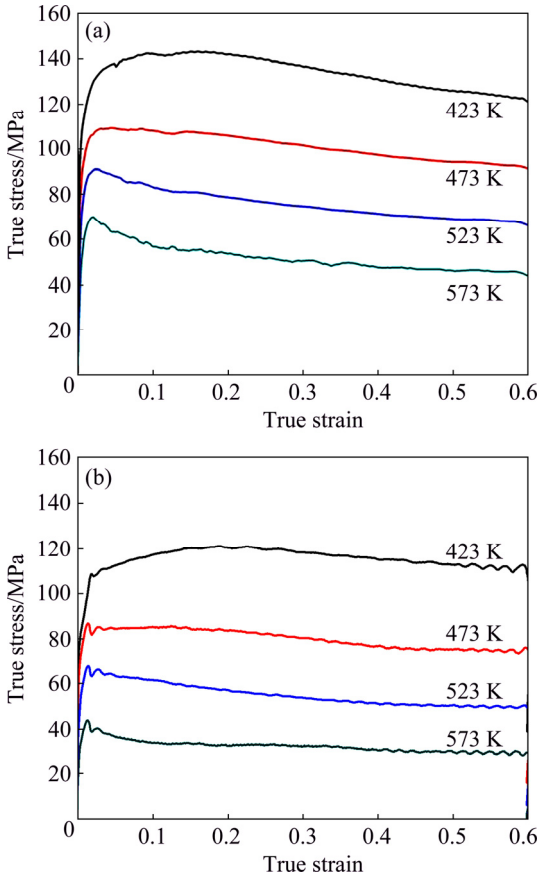

Fig. 6 Smoothed flow curves of Mg−9Li−3Al−2Sr alloy at different strain rates: (a) 1 s^{-1}; (b) 0.1 s^{-1}

The linear relationships of $\ln\dot{\varepsilon}-\ln[\sinh(\alpha\sigma)]$ at a given temperature and $\ln[\sinh(\alpha\sigma)]-1000/T$ at a strain rate were fitted as seen in Figs. 8 and 9. Take the mean value of all the slopes in Fig. 8, then Q_1=4.38118 kJ/mol, and the mean value of all the slopes in Fig. 9 is Q_2=3.02382 kJ/mol. Since $Q=RQ_1Q_2$, Q value of Mg−9Li−3Al−2Sr alloy is calculated as1 10.14 kJ/mol at a strain of 0.2. According to Eq. (10), the $\ln A-Q/(RT)$ is the intercept of the $\ln\dot{\varepsilon}-\ln[\sinh(\alpha\sigma)]$ curve in Fig. 8. $\ln A$ can be calculated at different temperatures, and the average value of $\ln A$ would be 22.3155. So, the material constant of A is 4.91×10^9.

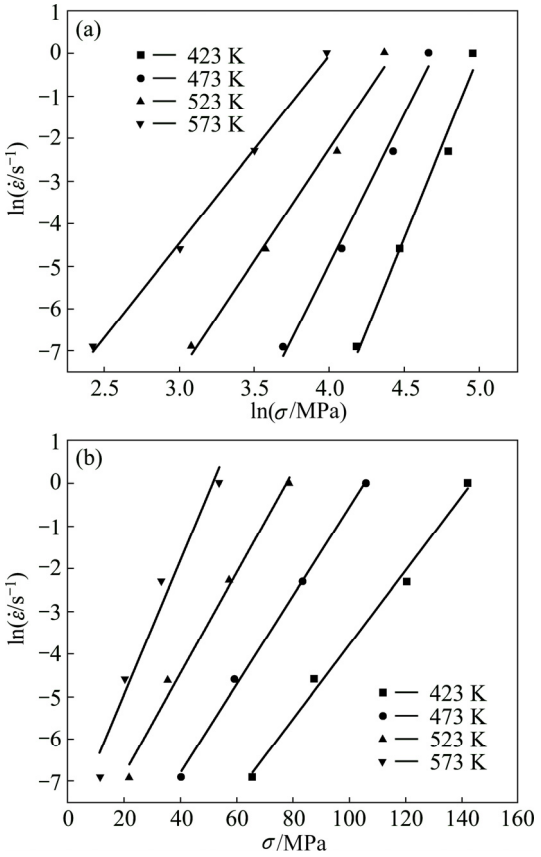

Fig. 7 $\ln\dot{\varepsilon}-\ln\sigma$ and $\ln\dot{\varepsilon}-\sigma$ relation curves at different temperatures

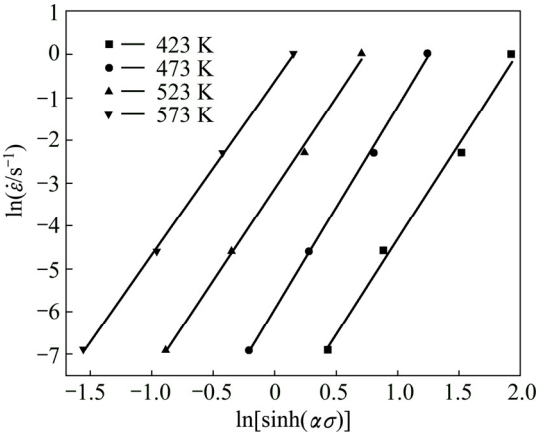

Fig. 8 $\ln\dot{\varepsilon}-\ln[\sinh(\alpha\sigma)]$ relation curves at different temperatures

The values of material constants (Q, $\ln A$, n and α) of the constitutive equations were computed at different deformation strains (0.1, 0.15, 0.2, 0.25, 0.3, 0.35, 0.4, 0.45, 0.5, 0.55). The relationships between different material constants and true strains can be determined

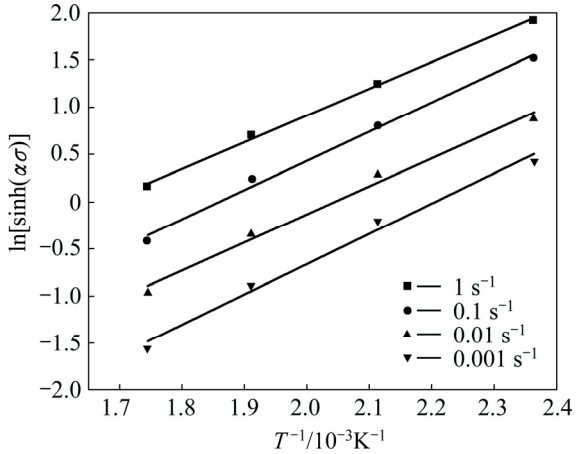

Fig. 9 ln[sinh($\alpha\sigma$)]−1000/T relation curves at different strain rates

using polynomial curve fitting as shown in Fig. 10. It is recognized that the sixth order polynomial gives a good fit to the calculated values in a wide range of strain levels. The expressions are shown in Eqs. (12)−(15) and the polynomial constants for Q, ln A, n and α are provided in Table 2.

$$\alpha = \alpha_1 + \alpha_2\varepsilon + \alpha_3\varepsilon^2 + \alpha_4\varepsilon^3 + \alpha_5\varepsilon^4 + \alpha_6\varepsilon^5 + \alpha_7\varepsilon^6 \quad (12)$$

$$\ln A = A_1 + A_2\varepsilon + A_3\varepsilon^2 + A_4\varepsilon^3 + A_5\varepsilon^4 + A_6\varepsilon^5 + A_7\varepsilon^6 \quad (13)$$

$$n = n_1 + n_2\varepsilon + n_3\varepsilon^2 + n_4\varepsilon^3 + +n_5\varepsilon^4 + n_6\varepsilon^5 + n_7\varepsilon^6 \quad (14)$$

$$Q = Q_1 + Q_2\varepsilon + Q_3\varepsilon^2 + Q_4\varepsilon^3 + Q_5\varepsilon^4 + Q_6\varepsilon^5 + Q_7\varepsilon^6 \quad (15)$$

Using Eq. (16), derived from Eqs. (1) and (7), the stress can be expressed in the Zenner−Hollomon form:

$$\sigma = \frac{1}{\alpha}\ln\left\{\left(\frac{Z}{A}\right)^{\frac{1}{n}} + \left[\left(\frac{Z}{A}\right)^{\frac{2}{n}} + 1\right]^{\frac{1}{2}}\right\} = \frac{1}{\alpha}\ln\left\{\left(\frac{\dot{\varepsilon}\exp(\frac{Q}{RT})}{A}\right)^{\frac{1}{n}} + \left[\left(\frac{\dot{\varepsilon}\exp(\frac{Q}{RT})}{A}\right)^{\frac{2}{n}} + 1\right]^{\frac{1}{2}}\right\} \quad (16)$$

In order to verify the developed constitutive model, comparisons between the predicted and experimental results were carried out as shown in Fig. 11. The proposed flow stress model gives a good estimate of the flow stress for Mg−9Li−3Al−2Sr alloy under most deformation conditions. However, some points deviate from the exact results. So, the proposed model can be used to numerically analyze the hot deformation

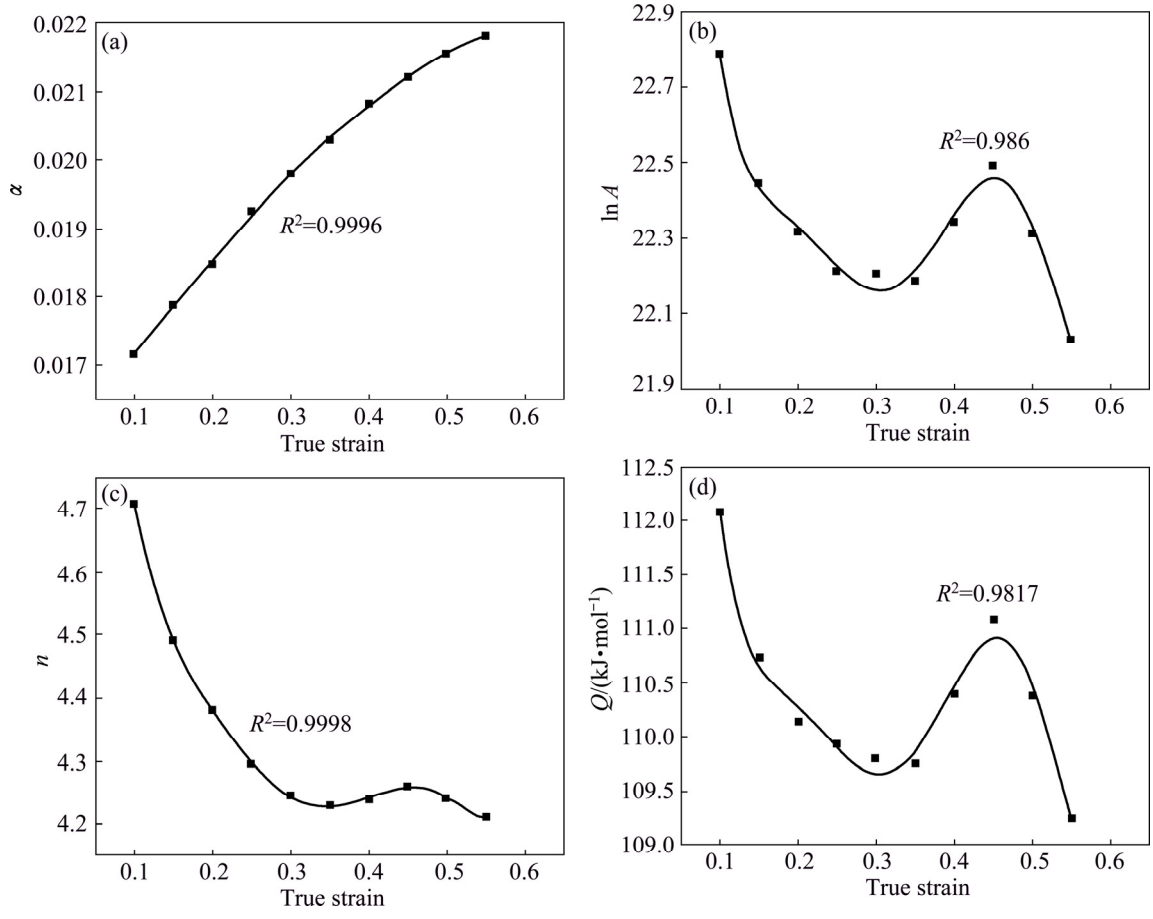

Fig. 10 Relationship between constants and true strains: (a) α; (b) ln A; (c) n; (d) Q

Table 2 Coefficients of polynomial functions

α	Value	A	Value	n	Value	Q/(kJ·mol^{-1})	Value
α_1	0.016	A_1	29.18	n_1	6.5904	Q_1	138.21
α_2	0.0097	A_2	−152.24	n_2	−39.921	Q_2	−620.69
α_3	0.0123	A_3	1399.8	n_3	325.69	Q_3	5678.2
α_4	0.096	A_4	−6641.6	n_4	−1468.1	Q_4	−26746
α_5	−0.6561	A_5	16814	n_5	3627.8	Q_5	67194
α_6	1.2608	A_6	−21404	n_6	−4562.6	Q_6	−84883
α_7	−0.8191	A_7	10722	n_7	2275.1	Q_7	42196

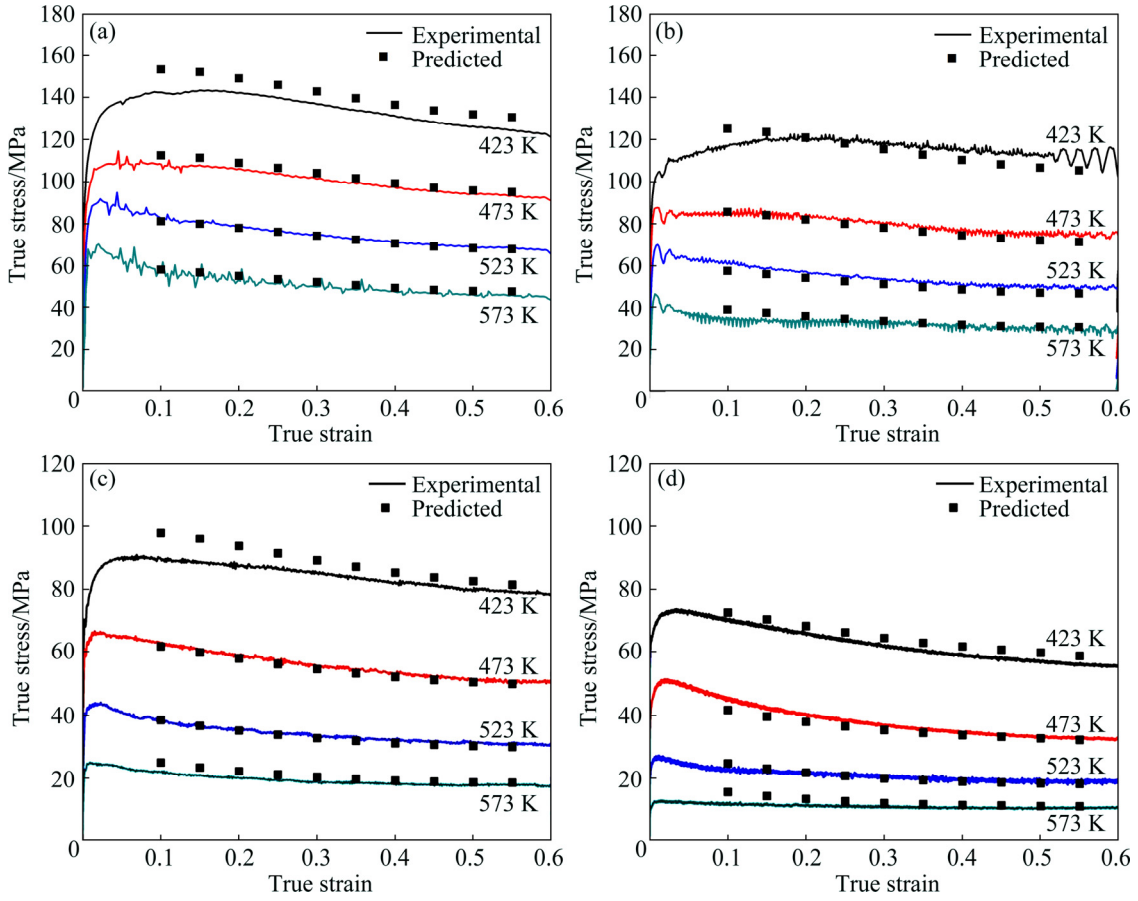

Fig. 11 Comparison of predicted and experimental values under different deformation conditions: (a) 1 s^{-1}; (b) 0.1 s^{-1}; (c) 0.01 s^{-1}; (d) 0.001 s^{-1}

processes. MEHTEDI et al [36,40] considered that the necking or barreling may influence accuracy of experimental dataset in compression or tension tests. The lubricants between the sample surface and anvil also bring about the non-uniform stress, especially in the high strain rate.

Figure 12 shows the comparison between the experimental and predicted results by the developed constitutive equations of Mg−9Li−3Al−2Sr alloy at different temperatures under strain rates of 0.001, 0.01, 0.1 and 1.0 s^{-1}. The standard statistical parameters such as correlation coefficient (R^2) and average absolute relative error (AARE) were used to quantify the predictability of the flow stress as shown in Eqs. (17) and (18) [18,37]:

$$R=\frac{\sum_{i=1}^{i=N}(\sigma_{\exp}^{i}-\bar{\sigma}_{\exp})(\sigma_{\mathrm{p}}^{i}-\bar{\sigma}_{\mathrm{p}})}{\sqrt{\sum_{i=1}^{i=N}(\sigma_{\exp}^{i}-\bar{\sigma}_{\exp})^2\sum_{i=1}^{i=N}(\sigma_{\mathrm{p}}^{i}-\bar{\sigma}_{\mathrm{p}})^2}} \tag{17}$$

$$\mathrm{AARE}=\frac{1}{N}\sum_{i=1}^{i=N}\left|\frac{\sigma_{\exp}^{i}-\sigma_{\mathrm{p}}^{i}}{\sigma_{\exp}^{i}}\right|\times 100\% \tag{18}$$

where $\sigma_{\exp}$ is the experimental flow stress and σ_{p} is the predicted flow stress obtained from the developed constitutive equation; $\bar{\sigma}_{\exp}$ and $\bar{\sigma}_{\mathrm{p}}$ are the mean values of $\sigma_{\exp}$ and σ_{p}, respectively; N is the total number of data points used in this study; R is a commonly employed statistical parameter and provides information on the

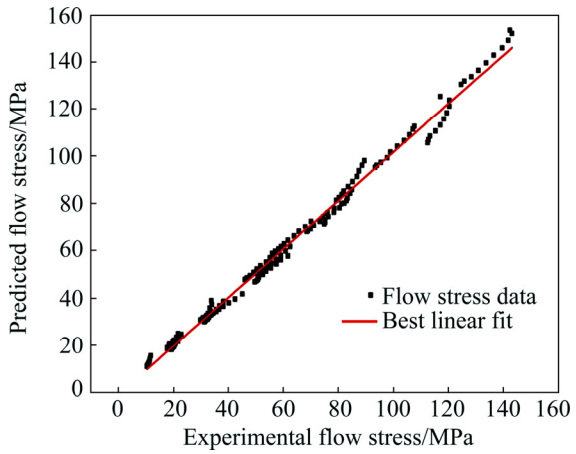

Fig. 12 Correlation between experimental and predicted flow stress data from developed constitutive equation

strength of the linear relationship between the experimental and predicted data [18,26,39]. R^2=0.9970 and AARE=4.41% are determined by the data at various strains (0.1−0.55) with intervals of 0.05 for the entire strain rate and temperature regime according to Eqs. (17) and (18), which reflected good prediction capabilities of the developed constitutive model. To validate the model for a more complicated deformation path, further Gleeble experiments were conducted such that the test specimen was deformed at one temperature and then quickly the strain rate was changed (Figs. 13(a) and (b)). Another test specimen was compressed at a strain rate of 0.02 s^{-1} during a continuous cooling test from 573 to 389 K (Figs. 13(c) and (d)). As shown in Fig. 13(a), the prediction of the Zener–Hollomon equation can trace the sudden changed deformation very well. In order to simulate a more realistic thermomechanical history, referring to Fig. 13(b), the constitutive model can predict the stress strain behavior for more complicated thermomechanical histories similar to what may occur in a production environment. The results indicate that the proposed deformation constitutive equation gives an accurate estimate of the flow stress for this alloy, and can be used to analyze the problems during forming and casting processes.

4 Conclusions

1) The true stress−strain curves of the duplex phase Mg−9Li−3Al−2Sr alloy were obtained by the compression tests at the temperatures of 423−573 K

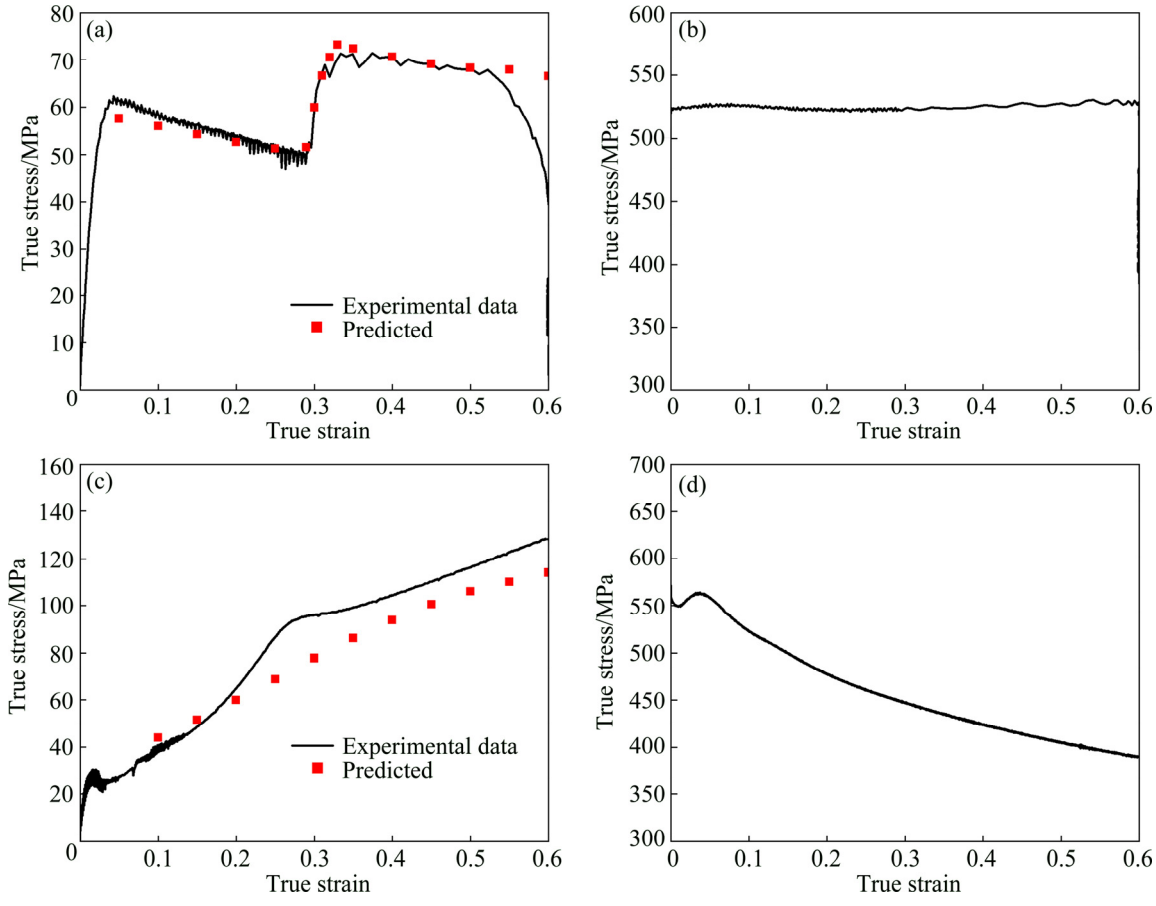

Fig. 13 Validation of model using new experimental data: (a) T=523 K, $\dot{\varepsilon}$=0.1 s^{-1} to a strain of 0.3 and then increased to $\dot{\varepsilon}$=1 s^{-1} to strain of 0.6; (b) Temperature condition experienced by compression sample of changed strain rates; (c) Continuous cooling test; (d) Temperature condition of continuous cooling test

and strain rates of 0.001−1 s^{-1}. At a certain strain, the flow stress increases with the decrease of deformation temperature and an increase of strain rate. Strain softening was seen at a critical strain and attributed to dynamic recovery and dynamic recrystallization.

2) Serrated flow was sensitive for this alloy in particular at low strain rates and was attributed to a dynamic strain aging (DSA) effect, the periodic shearing of dislocations by solute atoms Mg and Li in the duplex phase alloy.

3) The flow stress curves of Mg−9Li−3Al−2Sr alloy predicted by the developed Zener–Hollomon model are in good agreement with experimental results. The correlation coefficient and average absolute relative error (AARE) are 0.9970 and 4.41% respectively, which confirms the validity of the proposed model.

Acknowledgments

The authors would like to thank Mark WHITNEY for Gleeble test and Dr. Yu-quan DING for microstructure analysis in University of Waterloo.

References

[1] SLOOFF F A, ZHOU J, DUSZCZYK J, KATGERMAN L. Constitutive analysis of wrought magnesium alloy Mg−Al4−Zn1 [J]. Scripta Materialia, 2007, 57: 759−762.

[2] JIANG Bin, ZENG Ying, ZHANG Ming-xing, LIAO Ji-chao, PAN Fu-sheng. The effect of addition of cerium on the grain refinement of Mg−3Al−1Zn cast alloy [J]. Journal of Materials Research, 2013, 28: 2694−2700.

[3] XU Yan, HU Lian-xi, SUN Yu. Deformation behaviour and dynamic recrystallization of AZ61 magnesium alloy [J]. Journal of Alloys and Compounds, 2013, 580: 262−269.

[4] HUANG Y D, GAN W M, KAINER K U, HORT N. Role of multi-microalloying by rare earth elements in ductilization of magnesium alloys [J]. Journal of Magnesium and Alloys, 2014, 2(1): 1−7.

[5] WANG Lei, QIAO Qi, LIU Yang, SONG Xiu. Formability of AZ31 Mg alloy sheets within medium temperatures [J]. Journal of Magnesium and Alloys, 2013, 1(4): 312−317.

[6] MURALIDHAR A, NARENDRANATH S, SHIVANNANDA N H. Effect of equal channel angular pressing on AZ31 wrought magnesium alloys [J]. Journal of Magnesium and Alloys, 2013, 1(4): 336−340.

[7] TAKUDA H, MATSUSAKA H, KIKUCHI S, KUBOTA K. Tensile properties of a few Mg−Li−Zn alloy thin sheets [J]. Journal of Materials Science, 2002, 37: 51−57.

[8] DROZD Z, TROJANOVA Z, KUDELA S. Deformation behaviour of Mg−Li−Al alloys [J]. Journal of Alloys and Compounds, 2004, 378: 192−195.

[9] YANG Yan, PENG Xiao-dong, WEN Hai-ming, ZHENG Bao-long, ZHOU Yi-zhang, XIE Wei-dong. Influence of extrusion on the microstructure and mechanical behavior of Mg−9Li−3Al−*x*Sr alloys [J]. Metallurgical And Materials Transactions A — Physical Metallurgy and Materials Science A, 2013, 44: 1101−1113.

[10] JAIN C C, KOO C H. Creep behavior of extruded sheets of magnesium alloys containing La-rich mischmetal [J]. Materials Transactions, 2006, 47: 433−439.

[11] GAO L, YAN H, LUO J, ALAN A L, CHEN R S. Microstructure and mechanical properties of a high ductility Mg−Zn−Mn−Ce magnesium alloy [J]. Journal of Magnesium and Alloys, 2013, 1: 283−291.

[12] SINGH A, NAKAMURA M, WATANNBE M, KATO A, TSAI A P. Quasicrystal strengthened Mg−Zn−Y alloys by extrusion [J]. Scripta Materialia, 2003, 49: 417−422.

[13] WANG J Y, CHANG T C, CHANG L Z, LEE S. Effect of al and Mn content on the mechanical properties of various ECAE processed Mg−Li−Zn alloys [J]. Materials Transactions, 2006, 47: 971−976.

[14] KIM Y H, KIM J H, YU H S, CHOI J W, SON H T. Microstructure and mechanical properties of Mg−*x*Li−3Al−1Sn−0.4Mn alloys (*x*=5, 8 and 11wt%) [J]. Journal of Alloys and Compounds, 2014, 583: 15−20.

[15] WU Rui-zhi, QU Zhi-kun, ZHANG Mi-lin. Effects of the addition of Y in Mg−8Li−(1,3)Al alloy [J]. Materials Science and Engineering A, 2009, 516: 96−99.

[16] YANG Y, PENG X D, WEN H M, WEI G B, XIE W D, LAVERNIA E J. Microstructure and mechanical behavior of Mg−10Li−3Al−2.5Sr alloy [J]. Materials Science and Engineering A, 2014, 611: 1−8.

[17] LUO Xiao-ping, DANG Shue, KANG Li. Compression deformation behavior of AZ81 magnesium alloy at elevated temperatures [J]. Advances in Materials Science and Engineering, 2014, 2014: 1−7.

[18] HE An, CHEN Lin, HU Sheng, WANG Can. Constitutive analysis to predict high temperature flow stress in 20CrMo continuous casting billet [J]. Materials & Design, 2013, 46: 54−60.

[19] WEI G B, PENG X D, HADADZADEH A, MAHMOODKHANI Y, XIE W D, YANG Y. Constitutive modeling of Mg−9Li−3Al−2Sr−2Y at elevated temperatures [J]. Mechanics of Materials, 2015, 89: 241−253.

[20] HU Xiao-dong, JU Dong-ying. Application of Anand's constitutive model on twin roll casting process of AZ31 magnesium alloy [J]. Transactions of Nonferrous Metals Society of China, 2006, 16(S): s586−s590.

[21] TSENG S T, HU H T. Finite element verification on constitutive law of AZ31 magnesium alloy at 400 °C [J]. Transactions of Nonferrous Metals Society of China, 2013, 23(11): 3372−3382.

[22] YU Hui, YU Hua-shun, KIM Y, YOU Bong-sun, MIN Guang-hui. Hot deformation behavior and processing maps of Mg−Zn−Cu−Zr magnesium alloy [J]. Transactions of Nonferrous Metals Society of China, 2013, 23(3): 756−764.

[23] LV Bin-jiang, PENG Jian, SHI Da-wei, TANG Ai-tao, PAN Fu-sheng. Constitutive modeling of dynamic recrystallization kinetics and processing maps of Mg−2.0Zn−0.3Zr alloy based on true stress–strain curves [J]. Materials Science and Engineering A, 2013, 560: 727−733.

[24] QIN Yin-jiang, PAN Qing-lin, HE Yun-bin, LI Wen-bin, LIU Xiao-yan, FAN Xi. Modeling of flow stress for magnesium alloy during hot deformation [J]. Materials Science and Engineering A, 2010, 527: 2790−2797.

[25] TIAN Jun, SHI Zi-qiong. Creep mechanism and creep constitutive model of aluminum silicate short-fiber-reinforced magnesium matrix composite [J]. Transactions of Nonferrous Metals Society of China, 2014, 24(3): 632−640.

[26] LIN Yong-cheng, CHEN Ming-song, ZHONG Jue. Constitutive modeling for elevated temperature flow behavior of 42CrMo steel [J]. Computational Materials Science, 2008, 42: 470−477.

[27] LÜ Bin-jiang, PENG jian, WANG Yong-jian, AN Xiao-qin, ZHONG Li-ping, TANG Ai-tao. Dynamic recrystallization behavior and hot workability of Mg−2.0Zn−0.3Zr−0.9Y alloy by using hot compression test [J]. Materials & Design, 2014, 53: 357−365.

[28] NIE Jian-feng. The serrated flow behavior of Mg−Gd(−Mn−Sc) alloys [J]. Metallurgical and Materials Transactions A, 2009, 40: 2761−2771.

[29] NIE Jian-feng. Serrated flow and tensile properties of a Mg−Y−Nd alloy [J]. Scripta Materialia, 2004, 50: 51−55.
[30] CHATURVEDI M, LLOYD D J, TANGRI K. Serrated yielding in magnesium−10 wt.% silver alloy [J]. Metal Science, 1972, 6: 16−19.
[31] HAN En-hou. Investigations on the plastic instability in an HCP Mg−Li alloy [J]. Journal of Metallurgy, 2012, 2012: 1−5.
[32] WANG Cong, XU Yong-bo, HAN En-hou. Serrated flow and abnormal strain rate sensitivity of a magnesium–lithium alloy [J]. Materials Letters, 2006, 60: 2941−2944.
[33] COTTRELL A H. A note on the Portevin-Le Chatelier effect [J]. Philosophical Magazine, 1953, 44: 829−832.
[34] TIAN Bao-hui. Ageing effect on serrated flow in Al−Mg alloys [J]. Materials Science and Engineering A, 2003, 349: 272−278.
[35] PINK E. The effect of precipitates on characteristics of serrated flow in AlZn5Mg1 [J]. Acta Metallurgica, 1989, 37: 1773−1781.
[36] MEHTEDI M, MUSHARAVATI F, SPIGARELLI S. Modelling of the flow behaviour of wrought aluminium alloys at elevated temperatures by a new constitutive equation [J]. Materials & Design, 2014, 54: 869−873.
[37] CAI Jun, LI Fu-guo, LIU Tai-ying, CHEN Bo, HE Min. Constitutive equations for elevated temperature flow stress of Ti−6Al−4V alloy considering the effect of strain [J]. Materials & Design, 2011, 32: 1144−1151.
[38] CHEN Bin, ZHOU Wei-min, LI Song, LI Xiao-ling, LU Chen. Hot compression deformation behavior and processing maps of Mg−Gd−Y−Zr alloy [J]. Journal of Materials Engineering and Performance, 2013, 22: 2458−2466.
[39] QUAN Guo-zheng, LI Gui-sheng, CHEN Tao, WANG Yi-xin, ZHANG Yan-wei, ZHOU Jie. Dynamic recrystallization kinetics of 42CrMo steel during compression at different temperatures and strain rates [J]. Materials Science and Engineering A, 2011, 528: 4643−4651.
[40] SPIGARELLI S, MEHTEDI M. A new constitutive model for the plastic flow of metals at elevated temperatures [J]. Journal of Materials Engineering and Performance, 2013, 23: 658−665.

双相 Mg−Li 合金的热变形行为和本构模型

魏国兵[1]，彭晓东[1]，胡发平[1]，Amir HADADZADEH[2]，杨 艳[1]，谢卫东[1]，Mary A. WELLS[2]

1. 重庆大学 材料科学与工程学院，重庆 400044;
2. Mechanical and Mechatronics Engineering Department, University of Waterloo, Waterloo, ON, N2L 3G1, Canada

摘 要：在温度 423~573 K 和应变速率为 0.001~1 s^{-1} 下，通过 Gleeble−3500 热机械试验机对双相 Mg−9Li−3Al−2Sr 合金进行等温热压缩实验，研究其热变形行为并评估其可加工性能。塑性失稳以锯齿形流变的形式存在，锯齿屈服效应归因于 Mg 和 Li 原子对移动位错的锁定作用。分析流变应力、应变速率和变形温度的关系，并通过 Arrhenius 公式计算得到不同应变条件下变形激活能和基本的材料参数。温度和变形速率对合金变形行为的影响可以用 Zener–Hollomon 指数函数来表示。通过比较不同变形条件下的预测值与实验流变曲线，来验证本构方程的合理性。经计算，得到其相关系数为 0.9970，平均相对误差为 4.41%。结果表明，该本构模型可以准确地预测双相 Mg−9Li−3Al−2Sr 合金的高温变形流动行为。

关键词：本构模型；Mg−Li 合金；塑性失稳；Zener–Hollomon 参数

(Edited by Xiang-qun LI)